ELSEVIER

Contents lists available at ScienceDirect

Thin-Walled Structures

journal homepage: www.elsevier.com/locate/tws



Full length article

Three-dimensional nonlinear mixed 6-DOF beam element for thin-walled members



Xinlong Du, Jerome F. Hajjar*

Department of Civil and Environmental Engineering, Northeastern University, Boston, MA 02115, USA

ARTICLE INFO

Keywords: Corotational transformation Mixed element Hellinger-Reissner variational principle Axial-flexural-torsional interaction Shear center Fiber section

ABSTRACT

This paper presents a three-dimensional mixed beam element formulation for fully nonlinear distributed plasticity analysis of members composed of sections with no significant torsional warping such as steel angles and tees. This formulation is presented using a corotational total Lagrangian approach and implemented in the OpenSees corotational framework. In this context, a basic coordinate system is lined up with the element chord and translates and rotates as the element deforms. The element tangent stiffness matrix and resisting forces in the basic system are derived through linearization of the two-field Hellinger-Reissner variational principle. The displacement shape functions are cubic Hermitian functions for the transverse displacements and a linear shape function for the axial and torsional deformation. The generalized stress resultant shape functions are linear for moments and constant for axial force and torque with the P - δ effect considered, which are developed from equilibrium equations. The fiber section method with uniaxial constitutive laws is adopted to account for material nonlinearity. Since the degrees-of-freedom in the basic system are defined with respect to different reference points, all element responses are transformed to acting about the shear center before conducting the corotational transformation. The mixed element is validated through a number of experimental and numerical examples.

1. Introduction

The corotational framework has been widely used to address the geometric nonlinearity of three-dimensional beam elements [1–8]. Within the basic system that continuously translates and rotates with the element, the number of degrees-of-freedom (DOFs) are reduced since the rigid-body motions are separated and considered through the corotational transformation. The corotational transformation is independent of the element formulation in the basic system; therefore, for elements with the same number of nodes and DOFs, the mapping between the basic and global systems is the same. For the element development in the basic system, a geometrically linear formulation, a total Lagrangian formulation or an updated Lagrangian formulation cannot be employed [9]; however, the geometrically linear formulation cannot be used when the coupled flexural-torsional and axial-torsional deformations need to be considered.

Depending on what variables are regarded as the primary unknowns, the element formulations are classified as displacement-based, force-based, or mixed elements. Although the displacement-based element is considered the most straightforward to implement and efficient in computation, it has a significant limitation, in that the assumed shape functions can only represent a linear curvature distribution along the element length. In particular, a large number of displacement-based

elements are needed where highly nonlinear curvature occurs in plastic hinge regions [10,11]. In addition, if geometric nonlinearity is included in the basic system, displacement-based elements have a membrane locking problem when the element geometry becomes curved due to deformations. Force-based elements consider element end forces as primary unknowns, from which stress resultants along the element are obtained with the use of shape functions [7,12,13]. Equilibrium is strictly enforced, while compatibility is satisfied merely in a weighted average sense. As compared with displacement-based elements, forcebased elements often demand state determination procedures that are more computationally intensive [3]. Two-field mixed elements treat both displacements and element end forces as primary unknowns, which require shape functions for both internal stress resultants and deformations [14-16]. Both equilibrium and compatibility are satisfied in a weighted average sense. Despite the relative complexity of the state determination procedure, mixed elements can be used to model nonlinear curvature efficiently, and they can avoid membrane locking when high-order finite strain terms are included in the element formulation.

In the context of nonlinear analysis of members with generic cross sections, displacement-based elements have been developed using the updated Lagrangian formulation [17–21] and corotational total Lagrangian formulation [2–4,8,22]. Alsafadie et al. [23,24] published a

E-mail addresses: du.xinl@northeastern.edu (X. Du), jf.hajjar@northeastern.edu (J.F. Hajjar).

Corresponding author.

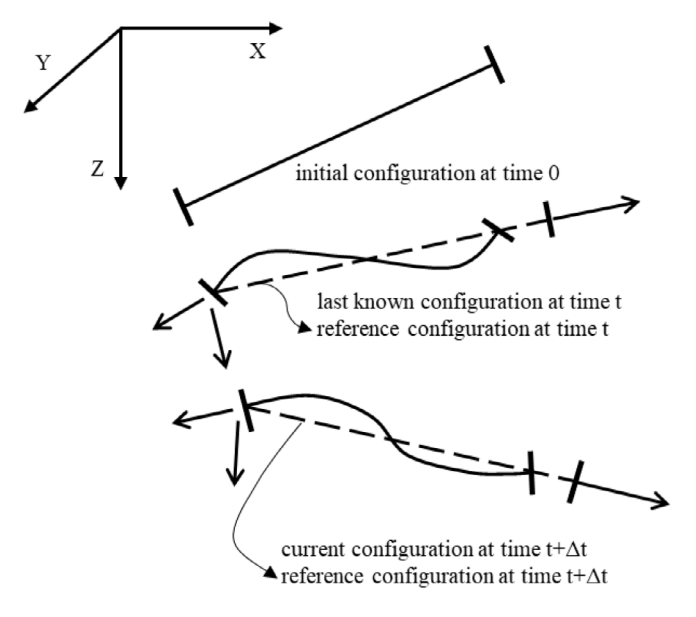


Fig. 1. Illustration of the corotational total Lagrangian formulation (after Mattiasson et al. [9]).

corotational mixed finite element formulation for thin-walled beams with generic cross sections. In this paper, a mixed beam element is developed within the corotational total Lagrangian framework. The proposed element adopts a different kinematic model from the one used by Alsafadie et al. [23,24], so that classical beam theory, where torsion is defined with respect to the shear center and bending is referred to the centroid, is satisfied. This kinematic model ensures that the axial, flexural and torsional deformations in the basic system are decoupled if the geometric nonlinear effects are not considered. Since in the present research bending and torsion are defined with respect to different reference points, all element responses are transformed to act about the shear center in order to conduct the corotational transformation. In addition, this element is developed to model a range of structures composed of sections with no significant torsional warping such as steel angles and tees. The in-plane cross section distortion and local buckling effects are also neglected. This means that this paper only focuses on coupled axial, flexural and torsional buckling for geometric nonlinear analysis. For material nonlinearity, a fiber section approach with uniaxial constitutive laws for the fibers is used.

2. Corotational total Lagrangian framework

In order to capture flexural-torsional, axial-torsional, and axial-flexural interaction behavior of members with asymmetric sections, the high-order terms in the Green-Lagrange strain are included through the total Lagrangian formulation in the basic system of the corotational transformation formulation. In the corotational transformation, when describing displacements and strains at time $t+\Delta t$, the reference system is the basic system at time $t+\Delta t$ (see Fig. 1). The element is formulated in the 6-DOF basic system at time $t+\Delta t$, and then transformed to the global system using the corotational transformation matrix at this time. The transformation matrix is different at different time points because the basic system continuously rotates and translates with the element. The deformational response is considered at the level of the basic system, whereas the rigid body motion is captured by the transformation matrix relating the basic and global systems. Therefore, there are only 6 DOFs in the basic system.

The displacements, forces and stiffnesses transformations between the basic and global systems that were implemented in OpenSees [25] are introduced here briefly. The tangential relation between the displacements \hat{D}_b in the basic system and the displacements \hat{D} in the global systems can be defined as

$$\delta \mathbf{D}_b = T \delta \hat{\mathbf{D}} \tag{1}$$

where T is a transformation matrix connecting the global and basic systems. Equating the internal virtual work in both the basic and global systems, the relationship between element end forces in the basic and global systems can be obtained as

$$\hat{\boldsymbol{P}} = \boldsymbol{T}^T \boldsymbol{P}_b \tag{2}$$

where \hat{P} and P_b are the element end forces at the global system and basic system, respectively. The element tangent stiffness matrix in the global system is obtained from the linearization of Eq. (2), such that

$$\delta \hat{\boldsymbol{P}} = \delta \left(\boldsymbol{T}^T \boldsymbol{P}_b \right) = \boldsymbol{T}^T \delta \boldsymbol{P}_b + \delta \boldsymbol{T}^T \boldsymbol{P}_b = \boldsymbol{T}^T \boldsymbol{K}_b \delta \boldsymbol{D}_b + \delta \boldsymbol{T}^T \boldsymbol{P}_b$$

$$= \left(\boldsymbol{T}^T \boldsymbol{K}_b \boldsymbol{T} + \boldsymbol{K}_G \right) \delta \hat{\boldsymbol{D}}$$

$$= \hat{\boldsymbol{K}} \delta \hat{\boldsymbol{D}}$$
(3)

where K_b is the tangent stiffness matrix in the basic system, and $\delta P_b = K_b \delta D_b$ is used in the above equation. Here,

$$\hat{K} = T^T K_b T + K_G \tag{4}$$

is the tangent stiffness matrix in the global system. The first term on the right hand side of Eq. (4) includes the contributions of the material stiffness matrix and the internal geometric stiffness matrix since in this research the total Lagrangian formulation is used to develop K_b , while the second term K_G is called the external geometric stiffness matrix. The detailed derivation of T and K_G is described by Crisfield [6] and de Souza [7]. When deriving the stiffness matrix and force recovery equation in the basic system, we can assume that the basic system is fixed and apply the total Lagrangian formulation in the basic system. This means that the Green-Lagrange strain tensor and the 2nd Piola-Kirchhoff stress tensor will be adopted to describe the element responses with respect to the reference configuration.

3. Mixed beam element in the basic system

This section presents the development of a new mixed beam element in the OpenSees framework, which can be used to simulate the geometrically and materially nonlinear behavior of members with asymmetric cross sections. The use of a mixed element results in a reduction of the number of elements required for nonlinear curvature problems with a comparable level of accuracy as compared to common displacement-based elements.

3.1. Coordinate systems for asymmetric sections

A thin-walled prismatic element with an asymmetric section is shown in Fig. 2. The basic system is defined by two set of coordinates: x, y, z and x, y, z. The coordinate system x, y, z is chosen such that x passes through the end cross section centroids C and C', and y and z are the section principal axes. A parallel set of coordinates x, y, z is chosen such that x passes through the end cross section shear centers S and S', and y and z are parallel to the principal y and z axes of the cross section. In this formulation, v and w denote the displacements of the shear center in the y and z directions, u the axial displacement along the centroidal axis CC', and ϕ the angle of twist about the shear center axis SS'. Such a coordinate system will uncouple axial, flexural and torsional deformations if the geometric nonlinear effects are not considered [18,19].

The element stiffness matrix is formulated in the basic system with 6 DOFs. The definitions of the DOFs are as follows: one relative axial displacement u_J of the centroids, two rotations relative to the chord θ_{Iy} and θ_{Jy} , about the y axis, two rotations relative to the chord θ_{Iz} and θ_{Jz} , about the z axis, and one relative angle of twist ϕ_J about the

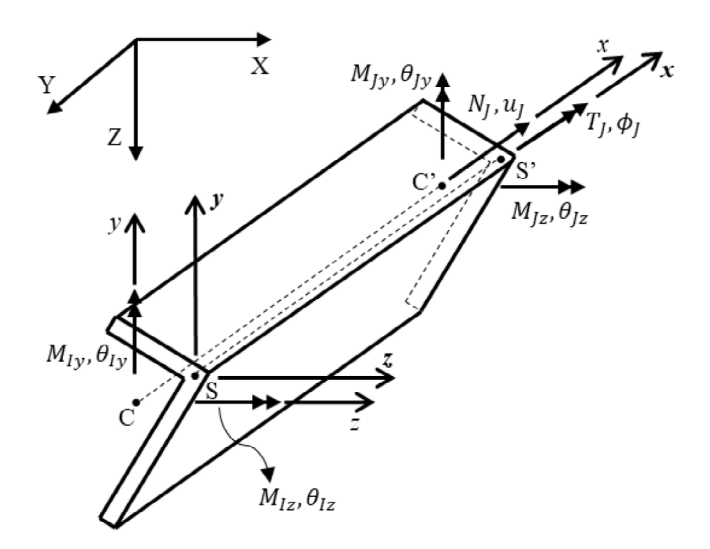


Fig. 2. Basic and global coordinate systems in space for asymmetric sections.

 \boldsymbol{x} axis. The statically independent element end forces corresponding to these displacements are: the axial force N_J acting along the centroidal axis CC'; the two bending moments acting about the principle axis z and in the \boldsymbol{xy} plane, M_{Iz} and M_{Jz} ; the two bending moments acting about the principle axis y and in the \boldsymbol{xz} plane, M_{Iy} and M_{Jy} ; and the torsional moment T_J acting about the shear center axis SS' [26]. These element end displacements and forces are gathered into vectors

$$\mathbf{D}_b = \begin{bmatrix} u_J & \theta_{Iz} & \theta_{Jz} & \theta_{Iy} & \theta_{Jy} & \phi_J \end{bmatrix}^T \tag{5}$$

and

$$\boldsymbol{P}_b = \begin{bmatrix} N_J & M_{Iz} & M_{Jz} & M_{Iy} & M_{Jy} & T_J \end{bmatrix}^T \tag{6}$$

Following the corotational transformation procedure, the forces, displacements and stiffness matrix need to be transformed to the global system. However, in the current definition of the basic system, some DOFs are defined with respect to the centroid, while others are defined with respect to the shear center, which means that the corotational transformation cannot be applied directly [22]. Consequently, all DOFs (end forces and displacements) need to be transformed to one reference point in advance of the corotational transformation. Note that in the basic system, the axial force is referred to the centroid, the lateral forces and torque are defined with respect to the shear center, and the moments act in the planes containing the shear center. Thus, it is straightforward to transform all DOFs to the shear center because only the axial force needs to be transformed. If other points (e.g., the centroid) are selected as the reference point, the lateral forces will need to be transformed, which is more difficult because the lateral forces will only be recovered after the corotational transformation. Therefore, it is appropriate to choose the shear center as the reference point and the shear center axis as the member reference axis before the corotational transformation. The coordinate system x, y, z is referred as the element basic reference system with the element end forces P_r and displacements D_r act through the shear center. The following equations are used to transform all DOFs to the shear center

$$\boldsymbol{P}_r = \boldsymbol{T}_{-}^T \boldsymbol{P}_b \tag{7}$$

$$D_b = T_r D_r \tag{8}$$

where the cross-sectional transformation matrix is [22]

$$T_r^T = \begin{bmatrix} 1 & 0 & 0 & 0 & 0 & 0 \\ y_s & 1 & 0 & 0 & 0 & 0 \\ -y_s & 0 & 1 & 0 & 0 & 0 \\ -z_s & 0 & 0 & 1 & 0 & 0 \\ z_s & 0 & 0 & 0 & 1 & 0 \\ 0 & 0 & 0 & 0 & 0 & 1 \end{bmatrix}$$

$$(9)$$

and y_s and z_s are coordinates of the shear center relative to the centroid. Consequently, the stiffness matrix in the element basic reference system is

$$K_r = T_{\star}^T K_h T_r \tag{10}$$

The corotational transformation will remain the same as in the original OpenSees with the Eqs. (1), (2) and (4) being modified as

$$\delta \mathbf{D}_r = T \delta \hat{\mathbf{D}} \tag{11}$$

$$\hat{\boldsymbol{P}} = \boldsymbol{T}^T \boldsymbol{P}_r \tag{12}$$

$$\hat{K} = T^T K_r T + K_G \tag{13}$$

3.2. Beam section kinematics

With the widely used kinematic assumption of the Euler-Bernoulli beam theory and ignoring the in-plane distortion behavior of the cross section, the motion of a material point P (x, y, z) (P is expressed in the coordinate system x, y, z shown in Fig. 2) on the beam section is expressed in terms of the displacements of the centroid and shear center [1,27]

$$u_p = u - yv' - zw' + z\phi v' - y\phi w'$$

$$v_p = v - \phi (z - z_s)$$

$$w_p = w + \phi (y - y_s)$$
(14)

where y_s and z_s are defined in Eq. (9); u, v, w and ϕ are defined in Section 3.1. The longitudinal/axial component of the Green-Lagrange strain is expressed as

$$\varepsilon = \frac{\partial u_p}{\partial x} + \frac{1}{2} \left(\frac{\partial u_p}{\partial x} \right)^2 + \frac{1}{2} \left(\frac{\partial v_p}{\partial x} \right)^2 + \frac{1}{2} \left(\frac{\partial w_p}{\partial x} \right)^2$$
 (15)

The high-order term $\frac{1}{2} \left(\partial u_p / \partial x \right)^2$ is negligible compared to $\partial u_p / \partial x$ because it is assumed that the term $\partial u_p / \partial x$ is small compared to unity. Hence, the Green-Lagrange strain becomes

$$\varepsilon = \frac{\partial u_p}{\partial x} + \frac{1}{2} \left(\frac{\partial v_p}{\partial x} \right)^2 + \frac{1}{2} \left(\frac{\partial w_p}{\partial x} \right)^2 \tag{16}$$

Taking derivatives of the displacement field in Eq. (14) with respect to x and substituting the results into Eq. (16) gives

$$\varepsilon = u' - yv'' - zw'' + \frac{1}{2} \left[(v')^2 + (w')^2 \right] + \frac{1}{2} \left[(y - y_s)^2 + (z - z_s)^2 \right] (\phi')^2 + (z_s v' - y_s w') \phi' + (zv'' - yw'') \phi$$
(17)

Compared with the strain term $\varepsilon = u' - yv'' - zw''$ used for the original OpenSees displacement-based element, Eq. (17) has the following extra terms

$$\frac{1}{2}\left[\left(v'\right)^2+\left(w'\right)^2\right]$$

$$\frac{1}{2}\left[\left(y-y_{s}\right)^{2}+\left(z-z_{s}\right)^{2}\right]\left(\phi'\right)^{2}$$

$$(z_sv'-y_sw')\phi'+(zv''-yw'')\phi$$

: geometric nonlinear term (coupling between the axial tension/compression and bending)

: Wagner term (coupling between the axial strain and torsion)

The shear strain at P resulting from uniform twisting ϕ' of a thinwalled open section member is approximated by [28]

$$\gamma = 2n\phi' \tag{18}$$

in which n is the perpendicular distance of point P (x, y, z) from the mid-thickness line of the cross section. Shear strains due to bending are neglected.

3.3. Displacement shape functions

In this formulation, the strain field is deduced from the nodal displacements \boldsymbol{D}_b in the basic system with the use of shape functions. Here all components of the stain vector obtained from displacement field \boldsymbol{D}_b are designated with a superposed hat. Thus, the combined strain vector as derived in Section 3.2 is shown as

$$\hat{\epsilon} = \begin{bmatrix} \hat{\epsilon} \\ \hat{\gamma} \end{bmatrix} = Y\hat{d} \tag{19}$$

where

$$Y = \begin{bmatrix} 1 & -y & z & (y - y_s)^2 + (z - z_s)^2 & 0 \\ 0 & 0 & 0 & 0 & 2n \end{bmatrix}$$
 (20)

and

$$\hat{d} = \begin{bmatrix} u' + \frac{1}{2} \left[(v')^2 + (w')^2 \right] + (z_s v' - y_s w') \phi' \\ v'' + w'' \phi \\ -w'' + v'' \phi \\ \frac{1}{2} (\phi')^2 \\ \phi' \end{bmatrix}$$
(21)

Vector \hat{d} is the cross section deformation vector. An infinitesimal change in \hat{e} can be written as

$$\delta \hat{\boldsymbol{\epsilon}} = \boldsymbol{Y} \delta \hat{\boldsymbol{d}} = \boldsymbol{Y} \boldsymbol{N}_{\delta \hat{d}_1} \boldsymbol{N}_{\delta \hat{d}_2} \delta \boldsymbol{D}_b \tag{22}$$

where the matrices ${\pmb N}_{\delta\hat d_1}$ and ${\pmb N}_{\delta\hat d_2}$ are

$$\boldsymbol{N}_{\delta\hat{d}1} = \begin{bmatrix} 1 & v' + z_s \phi' & w' - y_s \phi' & 0 & 0 & 0 & z_s v' - y_s w' \\ 0 & 0 & 0 & 1 & \phi & w'' & 0 \\ 0 & 0 & 0 & \phi & -1 & v'' & 0 \\ 0 & 0 & 0 & 0 & 0 & 0 & \phi' \\ 0 & 0 & 0 & 0 & 0 & 0 & 1 \end{bmatrix}$$
(23)

and

$$\mathbf{N}_{\delta\hat{d}_{2}} = \begin{bmatrix}
N'_{u1} & 0 & 0 & 0 & 0 & 0 \\
0 & N'_{v1} & N'_{v2} & 0 & 0 & 0 \\
0 & 0 & 0 & N'_{w1} & N'_{w2} & 0 \\
0 & N''_{v1} & N''_{v2} & 0 & 0 & 0 \\
0 & 0 & 0 & N''_{w1} & N''_{w2} & 0 \\
0 & 0 & 0 & 0 & N''_{w1} & N''_{w2} & 0 \\
0 & 0 & 0 & 0 & 0 & N_{\phi 1} \\
0 & 0 & 0 & 0 & 0 & N'_{\phi 1}
\end{bmatrix}$$
(24)

Here the shape functions are adopted to express the displacement field as the function of nodal displacements.

$$u = \mathbf{N}_{u}^{T} \mathbf{D}_{b} = \begin{bmatrix} N_{u1} & 0 & 0 & 0 & 0 \end{bmatrix} \mathbf{D}_{b}$$

$$v = \mathbf{N}_{v}^{T} \mathbf{D}_{b} = \begin{bmatrix} 0 & N_{v1} & N_{v2} & 0 & 0 & 0 \end{bmatrix} \mathbf{D}_{b}$$

$$w = \mathbf{N}_{w}^{T} \mathbf{D}_{b} = \begin{bmatrix} 0 & 0 & 0 & N_{w1} & N_{w2} & 0 \end{bmatrix} \mathbf{D}_{b}$$

$$\phi = \mathbf{N}_{b}^{T} \mathbf{D}_{b} = \begin{bmatrix} 0 & 0 & 0 & 0 & N_{b1} \end{bmatrix} \mathbf{D}_{b}$$
(25)

The shape functions in Eq. (25) are chosen as follows: cubic Hermitian functions for the transverse displacements, and a linear function for the axial and twist deformation. Specifically, the following shape functions are utilized in the current development

$$N_{u1} = \frac{x}{l_0}$$

$$N_{v1} = -N_{w1} = x \left(1 - \frac{x}{l_0}\right)^2$$

$$N_{v2} = -N_{w2} = x \left(\frac{x}{l_0}\right) \left(\frac{x}{l_0} - 1\right)$$

$$N_{\phi 1} = \frac{x}{l_0}$$
(26)

where l_0 is the length of the undeformed element.

3.4. Generalized stress resultant shape functions

The generalized stress resultant shape functions should be developed from the equilibrium equations, where the effects of torsion on the axial strains are neglected. Therefore, the strains at a material point P(x, y, z) on the beam section can be written in matrix form as

$$\tilde{\epsilon} = \begin{bmatrix} \tilde{\epsilon} \\ \tilde{\gamma} \end{bmatrix} = \tilde{Y}\tilde{d} \tag{27}$$

where

$$\tilde{d} = \begin{cases} u' + \frac{1}{2} \left[(v')^2 + (w')^2 \right] \\ v'' \\ -w'' \\ \phi' \end{cases}$$
 (28)

and

$$\tilde{Y} = \begin{bmatrix} 1 & -y & z & 0 \\ 0 & 0 & 0 & 2n \end{bmatrix} \tag{29}$$

In this section, variables with a superscript tilde mean that they are used to derive generalized stress resultant shape functions, and the other variables have the same meanings as defined in other sections. The principle of virtual work can be expressed as

$$\int_{L} \tilde{\boldsymbol{\delta}}^{T} \delta \tilde{\boldsymbol{d}} dx - \boldsymbol{P}_{b}^{T} \delta \boldsymbol{D}_{b} = 0$$
(30)

where the generalized stress resultant vector is

$$\tilde{S} = \begin{bmatrix} N \\ M_z \\ M_y \\ T \end{bmatrix}$$
(31)

and N, M_z , M_y and T are the axial force, the bending moment about z axis, the bending moment about y axis, and the St. Venant torque, respectively. The expanded form of the principle of virtual work is

$$\begin{split} &\int_{l_0} \left[N \left(\delta u' + v' \delta v' + w' \delta w' \right) + M_z \delta v'' - M_y \delta w'' + T \delta \phi' \right] dx - N_J \delta u_J \\ &- M_{Iz} \delta \theta_{Iz} - M_{Jz} \delta \theta_{Jz} - M_{Iy} \delta \theta_{Iy} - M_{Jy} \delta \theta_{Jy} - T_J \delta \phi_J = 0 \end{split}$$
 (32)

Eq. (32) is valid for all virtual displacements δu , δv , δw and $\delta \phi$ that satisfy the following essential boundary conditions [7]

$$\delta u\left(0\right) = \delta v\left(0\right) = \delta w\left(0\right) = \delta \phi\left(0\right) = \delta v\left(l_{0}\right) = \delta w\left(l_{0}\right) = 0 \tag{33}$$

Applying integration by parts and the essential boundary conditions to Eq. (32) gives

$$\begin{split} & \int_{l_0} \left\{ N' \delta u + \left[(Nv')' - M_z'' \right] \delta v + \left[(Nw')' + M_y'' \right] \delta w + T' \delta \phi \right\} dx \\ & + \left[-N \left(l_0 \right) + N_J \right] \delta u_J + \left[M_z(0) + M_{Iz} \right] \delta \theta_{Iz} \\ & + \left[-M_z \left(l_0 \right) + M_{Jz} \right] \delta \theta_{Jz} + \left[M_y(0) + M_{Iy} \right] \delta \theta_{Iy} \\ & + \left[-M_y \left(l_0 \right) + M_{Jy} \right] \delta \theta_{Jy} + \left[-T \left(l_0 \right) + T_J \right] \delta \phi_J = 0 \end{split}$$

$$(34)$$

During the derivation, the following relationships are used

$$u(l_{0}) = u_{J}, v'(0) = \theta_{Iz}, v'(l_{0}) = \theta_{Jz}, w'(0) = -\theta_{Iy}, w'(l_{0})$$

$$= -\theta_{Jy}, \phi(l_{0}) = \phi_{J}$$
(35)

Since Eq. (34) is satisfied for all admissible virtual displacements, the strong form of the governing equation can be obtained as [7]

$$\frac{dN}{dx} = 0$$

$$-\frac{d^2M_z}{dx} + \frac{d}{dx}\left(N\frac{dv}{dx}\right) = 0$$

$$\frac{d^2M_y}{dx} + \frac{d}{dx}\left(N\frac{dw}{dx}\right) = 0$$

$$\frac{dT}{dx} = 0$$
(36)

with the natural boundary conditions as below

$$\begin{split} N\left(l_{0}\right) &= N_{J}, M_{z}\left(0\right) = -M_{Iz}, M_{z}\left(l_{0}\right) = M_{Jz}, M_{y}\left(0\right) \\ &= -M_{Iy}, M_{y}\left(l_{0}\right) = M_{Jy}, T\left(l_{0}\right) \\ &= T_{J} \end{split} \tag{37}$$

The differential equations can be solved by integration with the natural boundary conditions. As such, the generalized stress resultant fields when the torsional deformation is uncoupled with flexural and axial deformations can be shown as

$$N(x) = N_{J}$$

$$M_{z}(x) = v(x) N_{J} + \left(\frac{x}{l_{0}} - 1\right) M_{Iz} + \frac{x}{l_{0}} M_{Jz}$$

$$M_{y}(x) = -w(x) N_{J} + \left(\frac{x}{l_{0}} - 1\right) M_{Iy} + \frac{x}{l_{0}} M_{Jy}$$

$$T(x) = T_{J}$$
(38)

This stress resultant field can be used as shape functions for the mixed element developed in this work. As for the Wagner stress resultant, a constant shape function is adopted [1,15]. Note that the P - δ effects are considered in the moment fields as $v(x) N_J$ and $-w(x) N_J$. This is because the geometric nonlinear term $\frac{1}{2} \left[\left(v' \right)^2 + \left(w' \right)^2 \right]$ is included

in the axial strain. Consequently, in the mixed element formulation in this work, when the beam element is subjected to end forces only, the generalized stress resultant internal force field within the element can be expressed as functions of end forces

$$S = \begin{bmatrix} N \\ M_z \\ M_y \\ W \\ T \end{bmatrix} = \begin{bmatrix} N_A & 0 & 0 & 0 & 0 & 0 & 0 \\ v & N_{z1} & N_{z2} & 0 & 0 & 0 & 0 \\ -w & 0 & 0 & N_{y1} & N_{y2} & 0 & 0 \\ 0 & 0 & 0 & 0 & 0 & N_W \\ 0 & 0 & 0 & 0 & 0 & N_T & 0 \end{bmatrix} \begin{bmatrix} N_J \\ M_{Iz} \\ M_{Jz} \\ M_{Iy} \\ T \\ W \end{bmatrix}$$
(39)

or

$$S = N_{D1} P_{c} \tag{40}$$

where W is the Wagner stress resultant. P_s is the generalized force degrees-of-freedom, in which both the nodal St. Venant torque T and the nodal Wagner stress resultant W contribute to the total nodal torque T_J [29]. For the stress resultant fields, a linear shape function for the moments and a constant shape for the axial force, torque and the Wagner field are adopted as

$$N_{z1} = N_{y1} = \frac{x}{l_0} - 1$$

$$N_{z2} = N_{y2} = \frac{x}{l_0}$$
(41)

$$N_A = N_W = N_T = 1$$

Note that the P - δ effects are included in the element internal moment fields with the use of the interpolated lateral displacements ν and w. These high order moments have significant impact on the moment distribution within an element because the assumption of a linear moment field is not accurate when the axial loads are relatively large. The variation of S is needed for the following derivations; thus, we have

$$\delta S = \delta N_{D1} P_s + N_{D1} \delta P_s = N_{D1} \delta P_s + N_{D2} \delta D_b$$
(42)

where the matrix N_{D2} is defined as

3.5. Cross section constitutive relations

Unlike the stress resultant vector S obtained from element end forces, the stress resultant vector S_{Σ} is derived from the strain vector $\epsilon = [\epsilon \ \gamma]^T$ through the constitutive law at the cross-sectional level. The nonlinear relationship between cross section resultants and cross section deformations can be obtained by taking integration of the constitutive laws over the cross section. Thus

$$S_{\Sigma} = \int_{A_0} Y^T \sigma(\epsilon) dA \tag{44}$$

where $\sigma = \begin{bmatrix} \sigma & \tau \end{bmatrix}^T$ is the corresponding stress vector, and A_0 is the cross section area of the undeformed element. The section tangent stiffness matrix is obtained by linearization of the cross-sectional constitutive relations with the use of $\epsilon = Yd$, where d is the cross section

deformation vector, as shown below

$$K_{s} = \frac{\partial S_{\Sigma}}{\partial d} = \int_{A_{0}} \mathbf{Y}^{T} \mathbf{E} \mathbf{Y} dA$$

$$= \int_{A_{0}} \begin{bmatrix} E & -yE & zE & p^{2}E & 0\\ -yE & y^{2}E & -yzE & -p^{2}yE & 0\\ zE & -yzE & z^{2}E & p^{2}zE & 0\\ p^{2}E & -p^{2}yE & p^{2}zE & p^{4}E & 0\\ 0 & 0 & 0 & 0 & 4n^{2}G \end{bmatrix} dA$$
(45)

in which

$$p^{2} = (y - y_{s})^{2} + (z - z_{s})^{2}$$
(46)

and matrix \boldsymbol{E} represents the constitutive relations of stresses and strains as shown

$$E = \begin{bmatrix} E & 0 \\ 0 & G \end{bmatrix} \tag{47}$$

where E is the tangent Young's modulus and G is the shear modulus. Furthermore, at the cross-sectional level, the following equality needs to be enforced: $S_{\Sigma} = S$, where S is obtained by the force interpolations through Eq. (39). In accounting for the material nonlinearity effects, the cross section is discretized into a grid of fibers and the section stiffness matrix K_s is computed using numerical integration. In this research, it is assumed that the uniform torsion behavior is linear elastic so that the shear strain is always elastic. Therefore, a uniaxial constitutive law is used to check the yielding of each fiber and update the tangent Young's modulus E as the fiber reaches plastic stage, while the shear modulus G remains constant. This means that the proposed element is only suitable for slender members with small shear deformations when it is used to model material nonlinearity.

3.6. Variational formulation

The mixed element formulation can be derived from the Hellinger-Reissner functional, which is a two-field functional of stresses and displacements. Here only end forces P_{ext} on the elements are considered. This principle is expressed as [1,14,15,30]

$$\delta \boldsymbol{D}_{b}^{T} \left\{ \int_{l_{0}} \boldsymbol{N}_{\delta \hat{\boldsymbol{d}} 2}^{T} \boldsymbol{N}_{\delta \hat{\boldsymbol{d}} 1}^{T} \boldsymbol{S} dx - \boldsymbol{P}_{ext} \right\} + \int_{l_{0}} \delta \boldsymbol{S}^{T} \left(\hat{\boldsymbol{d}} - \boldsymbol{d} \right) dx = 0$$
 (48)

where \hat{d} is the cross section deformation vector derived from displacement, and d is the cross section deformation vector derived from the interpolated generalized stress resultants. The first term of Eq. (48) represents the weak form of the equilibrium relations, and the second term represents the weak form of the strain compatibility relations. After Eq. (42) is substituted to Eq. (48)

$$\delta \boldsymbol{D}_{b}^{T} \left\{ \int_{l_{0}} \boldsymbol{N}_{\delta \hat{d}2}^{T} \boldsymbol{N}_{\delta \hat{d}1}^{T} \boldsymbol{S} dx + \int_{l_{0}} \boldsymbol{N}_{D2}^{T} \left(\hat{\boldsymbol{d}} - \boldsymbol{d} \right) dx - \boldsymbol{P}_{ext} \right\}$$

$$+ \delta \boldsymbol{P}_{s}^{T} \left\{ \int_{l_{0}} \boldsymbol{N}_{D1}^{T} \left(\hat{\boldsymbol{d}} - \boldsymbol{d} \right) dx \right\} = 0$$

$$(49)$$

Since $\delta {m D}_b^T$ and $\delta {m P}_s^T$ are arbitrary variations in corresponding state variables, Eq. (49) yields two sets of equations

$$\mathbf{g} = \int_{I_0} \mathbf{N}_{\delta \hat{d}^2}^T \mathbf{N}_{\delta \hat{d}^1}^T \mathbf{S} dx + \int_{I_0} \mathbf{N}_{D^2}^T (\hat{\boldsymbol{d}} - \boldsymbol{d}) dx - \boldsymbol{P}_{ext} = \mathbf{0}$$
 (50)

$$V = \int_{l_0} N_{D1}^T (\hat{d} - d) dx = 0$$
 (51)

where g and V represent the element equilibrium and strain-displacement compatibility vectors, respectively. In addition, noting the section equilibrium, a third equation is obtained as

$$U = S_{\Sigma} - S = 0 \tag{52}$$

where S_{Σ} denotes the generalized stress resultant vector obtained from the strain driven constitutive equations and S represents the interpolated generalized stress resultant vector.

3.7. Consistent linearization

Eq. (50)–(52) should be linearized consistently to obtain the element tangent stiffness matrix and other relations used in the element state determination procedure. Such a linearization process can be achieved by expanding the governing equations at the $(i+1)^{th}$ iteration based on the previous configuration at the i^{th} iteration.

3.7.1. Linearization of the section equilibrium equation

Through expanding the section equilibrium equation U = 0 about the configuration at the ith iteration while holding S constant, the following is obtained

$$U^{i+1} \approx U^{i} + \frac{\partial U}{\partial d} \Delta d = U^{i} + K_{s} \Delta d = 0$$
 (53)

or

$$\Delta d = -fU^i \tag{54}$$

where the section flexibility matrix f can be obtained by inverting the section stiffness matrix, i.e., $f = K_s^{-1}$.

3.7.2. Linearization of the element compatibility equation

The element compatibility equation $V(D_b, P_s) = 0$ should be expanded about the configuration at the i^{th} iteration in the element tangent stiffness formulation and element state determination process. Therefore, the result of a Taylor series expansion is given as follows

$$\boldsymbol{V}^{i+1} \approx \boldsymbol{V}^{i} + \frac{\partial \boldsymbol{V}}{\partial \boldsymbol{D}_{b}} \Delta \boldsymbol{D}_{b} + \frac{\partial \boldsymbol{V}}{\partial \boldsymbol{P}_{s}} \Delta \boldsymbol{P}_{s} = \boldsymbol{0}$$
 (55)

Further expansion of the second term on the right-hand side of Eq. (55) is written as

$$\frac{\partial \boldsymbol{V}}{\partial \boldsymbol{D}_{b}} \Delta \boldsymbol{D}_{b} \\
= \left[\int_{l_{0}} \frac{\partial \boldsymbol{N}_{D1}^{T}}{\partial \boldsymbol{D}_{b}} \left(\hat{\boldsymbol{d}} - \boldsymbol{d} \right) dx + \int_{l_{0}} \boldsymbol{N}_{D1}^{T} \frac{\partial \hat{\boldsymbol{d}}}{\partial \boldsymbol{D}_{b}} dx - \int_{l_{0}} \boldsymbol{N}_{D1}^{T} \frac{\partial \boldsymbol{d}}{\partial \boldsymbol{D}_{b}} dx \right] \Delta \boldsymbol{D}_{b} \\
= \left(\boldsymbol{M}_{d} + \boldsymbol{G}_{1} - \boldsymbol{H}_{12} \right) \Delta \boldsymbol{D}_{b} \tag{56}$$

where

$$G_{1} = \int_{l_{0}} N_{D1}^{T} \frac{\partial \hat{\boldsymbol{d}}}{\partial \boldsymbol{D}_{b}} dx = \int_{l_{0}} N_{D1}^{T} N_{\delta \hat{\boldsymbol{d}} 1} N_{\delta \hat{\boldsymbol{d}} 2} dx$$

$$(57)$$

$$H_{12} = \int_{l_{0}} N_{D1}^{T} \frac{\partial \boldsymbol{d}}{\partial \boldsymbol{D}_{b}} dx = \int_{l_{0}} N_{D1}^{T} \frac{\partial \boldsymbol{d}}{\partial \boldsymbol{S}_{\Sigma}} \frac{\partial \boldsymbol{S}_{\Sigma}}{\partial \boldsymbol{S}} \frac{\partial \boldsymbol{S}}{\partial \boldsymbol{D}_{b}} dx = \int_{l_{0}} N_{D1}^{T} \boldsymbol{f} N_{D2} dx$$

$$(58)$$

Here, $(\hat{a} - d)$ [2] and $(\hat{a} - d)$ [3] denote the second and the third terms of the vector $(\hat{a} - d)$, respectively. The third term on the right-hand side of Eq. (55) can be expressed as

$$\frac{\partial \mathbf{V}}{\partial \mathbf{P}_{s}} \Delta \mathbf{P}_{s}
= \left[\int_{l_{0}} \frac{\partial \mathbf{N}_{D1}^{T}}{\partial \mathbf{P}_{s}} (\hat{\mathbf{d}} - \mathbf{d}) dx + \int_{l_{0}} \mathbf{N}_{D1}^{T} \frac{\partial \hat{\mathbf{d}}}{\partial \mathbf{P}_{s}} dx - \int_{l_{0}} \mathbf{N}_{D1}^{T} \frac{\partial \mathbf{d}}{\partial \mathbf{P}_{s}} dx \right] \Delta \mathbf{P}_{s}
= -\mathbf{H}_{11} \Delta \mathbf{P}_{s}$$

(60)

with

$$\boldsymbol{H}_{11} = \int_{l_0} \boldsymbol{N}_{D1}^T \frac{\partial \boldsymbol{d}}{\partial \boldsymbol{P}_s} dx = \int_{l_0} \boldsymbol{N}_{D1}^T \frac{\partial \boldsymbol{d}}{\partial \boldsymbol{S}_{\Sigma}} \frac{\partial \boldsymbol{S}_{\Sigma}}{\partial \boldsymbol{S}} \frac{\partial \boldsymbol{S}}{\partial \boldsymbol{P}_s} dx = \int_{l_0} \boldsymbol{N}_{D1}^T \boldsymbol{f} \boldsymbol{N}_{D1} dx$$
(61)

Hence, Eq. (55) becomes

$$V^{i+1} \approx V^{i} + (M_d + G_1 - H_{12}) \Delta D_b - H_{11} \Delta P_s = 0$$
 (62)

and solving this equation for ΔP_{c} gives

$$\Delta P_{s} = H_{11}^{-1} \left(M_{d} + G_{1} - H_{12} \right) \Delta D_{b} + H_{11}^{-1} V^{i}$$
(63)

3.7.3. Linearization of the element equilibrium equation

A similar process is used for the linearization of the element equilibrium equation, which gives

$$\mathbf{g}^{i+1} \approx \mathbf{g}^{i} + \frac{\partial \mathbf{g}}{\partial \mathbf{D}_{b}} \Delta \mathbf{D}_{b} + \frac{\partial \mathbf{g}}{\partial \mathbf{P}_{c}} \Delta \mathbf{P}_{s} - \Delta \mathbf{P}_{ext} = \mathbf{0}$$
 (64)

Expansion of the second term on the right-hand side of Eq. (64) gives

$$\frac{\partial \mathbf{g}}{\partial \mathbf{D}_{b}} \Delta \mathbf{D}_{b}
= \left[\int_{l_{0}} \frac{\partial \mathbf{N}_{\delta d2}^{T}}{\partial \mathbf{D}_{b}} \mathbf{N}_{\delta d1}^{T} \mathbf{S} dx + \int_{l_{0}} \mathbf{N}_{\delta d2}^{T} \frac{\partial \mathbf{N}_{\delta d1}^{T}}{\partial \mathbf{D}_{b}} \mathbf{S} dx + \int_{l_{0}} \mathbf{N}_{\delta d2}^{T} \mathbf{N}_{\delta d1}^{T} \frac{\partial \mathbf{S}}{\partial \mathbf{D}_{b}} dx \right]
+ \int_{l_{0}} \frac{\partial \mathbf{N}_{D2}^{T}}{\partial \mathbf{D}_{b}} (\hat{\mathbf{d}} - \mathbf{d}) dx + \int_{l_{0}} \mathbf{N}_{D2}^{T} \frac{\partial \hat{\mathbf{d}}}{\partial \mathbf{D}_{b}} dx - \int_{l_{0}} \mathbf{N}_{D2}^{T} \frac{\partial \mathbf{d}}{\partial \mathbf{D}_{b}} dx \right] \Delta \mathbf{D}_{b}
= (\mathbf{K}_{g} + \mathbf{G}_{2}^{T} + \mathbf{G}_{2} - \mathbf{H}_{22}) \Delta \mathbf{D}_{b}$$
(65)

where

$$G_2 = \int_{l_0} \mathbf{N}_{D2}^T \mathbf{N}_{\delta \hat{d}1} \mathbf{N}_{\delta \hat{d}2} dx \tag{66}$$

$$\boldsymbol{H}_{22} = \int_{I_0} \boldsymbol{N}_{D2}^T \boldsymbol{f} \, \boldsymbol{N}_{D2} dx \tag{67}$$

$$\mathbf{K}_{g} = \int_{I_{0}} \mathbf{N}_{\delta \hat{d}2}^{T} \mathbf{G} \mathbf{N}_{\delta \hat{d}2} dx \tag{68}$$

in which

$$G = \begin{bmatrix} 0 & 0 & 0 & 0 & 0 & 0 & 0 & 0 \\ 0 & N & 0 & 0 & 0 & 0 & Nz_s \\ 0 & 0 & N & 0 & 0 & 0 & -Ny_s \\ 0 & 0 & 0 & 0 & 0 & M_y & 0 \\ 0 & 0 & 0 & 0 & 0 & M_z & 0 \\ 0 & 0 & 0 & M_y & M_z & 0 & 0 \\ 0 & Nz_s & -Ny_s & 0 & 0 & 0 & W \end{bmatrix}$$
 (69)

The third term on the right-hand side of Eq. (64) is

$$\frac{\partial \mathbf{g}}{\partial \mathbf{P}_{s}} \Delta \mathbf{P}_{s}
= \left[\int_{l_{0}} \frac{\partial \mathbf{N}_{\delta \hat{d}2}^{T}}{\partial \mathbf{P}_{s}} \mathbf{N}_{\delta \hat{d}1}^{T} \mathbf{S} dx + \int_{l_{0}} \mathbf{N}_{\delta \hat{d}2}^{T} \frac{\partial \mathbf{N}_{\delta \hat{d}1}^{T}}{\partial \mathbf{P}_{s}} \mathbf{S} dx + \int_{l_{0}} \mathbf{N}_{\delta \hat{d}2}^{T} \mathbf{N}_{\delta \hat{d}1}^{T} \frac{\partial \mathbf{S}}{\partial \mathbf{P}_{s}} dx \right]
+ \int_{l_{0}} \frac{\partial \mathbf{N}_{D2}^{T}}{\partial \mathbf{P}_{s}} (\hat{\mathbf{d}} - \mathbf{d}) dx + \int_{l_{0}} \mathbf{N}_{D2}^{T} \frac{\partial \hat{\mathbf{d}}}{\partial \mathbf{P}_{s}} dx - \int_{l_{0}} \mathbf{N}_{D2}^{T} \frac{\partial \mathbf{d}}{\partial \mathbf{P}_{s}} dx \right] \Delta \mathbf{P}_{s}
= (\mathbf{G}_{1} + \mathbf{M}_{d} - \mathbf{H}_{12})^{T} \Delta \mathbf{P}_{s} \tag{70}$$

Hence, Eq. (64) becomes

$$g^{i+1} \approx g^{i} + \left(K_g + G_2^T + G_2 - H_{22}\right) \Delta D_b$$

$$+ \left(G_1 + M_d - H_{12}\right)^T \Delta P_s - \Delta P_{ext} = 0$$
(71)

3.7.4. Consistent element tangent stiffness matrix

Substituting ΔP_{c} from Eq. (63) to Eq. (71) shows that

$$g^{i} + (K_{g} + G_{2}^{T} + G_{2} - H_{22}) \Delta D_{b}$$

$$+ (G_{1} + M_{d} - H_{12})^{T} H_{11}^{-1} (M_{d} + G_{1} - H_{12}) \Delta D_{b}$$

$$+ (G_{1} + M_{d} - H_{12})^{T} H_{11}^{-1} V^{i} - \Delta P_{ext} = 0$$
(72)

Solving the above equation for ΔD_b and employing the definition of g at the i^{th} iteration give us

$$\begin{aligned}
& \left[\left(\mathbf{K}_{g} + \mathbf{G}_{2}^{T} + \mathbf{G}_{2} - \mathbf{H}_{22} \right) \\
&+ \left(\mathbf{G}_{1} + \mathbf{M}_{d} - \mathbf{H}_{12} \right)^{T} \mathbf{H}_{11}^{-1} \left(\mathbf{M}_{d} + \mathbf{G}_{1} - \mathbf{H}_{12} \right) \right] \Delta \mathbf{D}_{b} \\
&= - \int_{l_{0}} \mathbf{N}_{\delta d2}^{T} \mathbf{N}_{\delta d1}^{T} \mathbf{S}^{i} dx - \int_{l_{0}} \mathbf{N}_{D2}^{T} \left(\hat{\mathbf{d}}^{i} - \mathbf{d}^{i} \right) dx + \mathbf{P}_{ext}^{i} \\
&- \left(\mathbf{G}_{1} + \mathbf{M}_{d} - \mathbf{H}_{12} \right)^{T} \mathbf{H}_{11}^{-1} \mathbf{V}^{i} + \Delta \mathbf{P}_{ext}
\end{aligned} \tag{73}$$

or in a compact form

$$\mathbf{K}_{b}\Delta \mathbf{D}_{b} = \mathbf{P}_{ext}^{i+1} - \mathbf{P}_{int}^{i} \tag{74}$$

where the tangent stiffness matrix K_b and the internal force vector P^i_{int} are given as

$$\mathbf{K}_{b} = \left(\mathbf{K}_{g} + \mathbf{G}_{2}^{T} + \mathbf{G}_{2} - \mathbf{H}_{22}\right) \\
+ \left(\mathbf{G}_{1} + \mathbf{M}_{d} - \mathbf{H}_{12}\right)^{T} \mathbf{H}_{11}^{-1} \left(\mathbf{G}_{1} + \mathbf{M}_{d} - \mathbf{H}_{12}\right) \\
\mathbf{P}_{int}^{i} = \mathbf{G}_{1}^{T} \mathbf{P}_{s}^{i} + \int_{\mathbf{D}_{2}} \mathbf{N}_{D2}^{T} \left(\hat{\mathbf{d}}^{i} - \mathbf{d}^{i}\right) dx + \left(\mathbf{G}_{1} + \mathbf{M}_{d} - \mathbf{H}_{12}\right)^{T} \mathbf{H}_{11}^{-1} \mathbf{V}^{i} \tag{76}$$

and we have

$$\boldsymbol{P}_{oxt}^{i+1} = \boldsymbol{P}_{oxt}^{i} + \Delta \boldsymbol{P}_{oxt} \tag{77}$$

Note that the first part of K_b is the element internal geometric stiffness matrix and the second part is the element material stiffness matrix.

3.8. Element state determination

Once the incremental displacements and rotations are retrieved from the global solution, the element state determination process is started by updating the nodal displacements and rotations in the global system and then computing the rotations and the axial displacement in the basic system through the corotational transformation. For the steps related to calculating the new state for the element in the basic system, the following descriptions should apply.

Different approaches of element state determination can be adopted based on the three nonlinear governing equations (Eqs. (50)-(52)). An iteration method should be used to solve the global equilibrium equation. As for the section equilibrium and element compatibility, nonlinear iterations can be performed prior to returning to higher level, or linearized equations may be used and the residuals at these levels may be pushed to the global level and then removed by global iterations [30,31]. Compared to the linearized approximation option, the nonlinear iteration option commonly needs fewer global iterations at the cost of more intensive computations at the section or element level and is advantageous for cases in which inelasticity is concentrated in only a few elements [30]. In this research, as in that of others [14,31,32], the linearized approximation option is utilized at both the section and element levels. Once the trial displacements D_h^{i+1} in the basic system are obtained from last converged state, the following element state determination procedure is adopted to calculate the tangent stiffness matrix and do force recovery in the basic system.

- 1. Calculate section deformation \hat{d}^{i+1} at each Gauss point (use displacement shape functions) from Eq. (21).
- 2. Update the generalized force degrees-of-freedom (nodal forces) using $P_s^{t+1} = P_s^t + \Delta P_s$ with ΔP_s calculated from Eq. (63).
- 3. Calculate the generalized stress resultant shape functions from Eqs. (39), (40) and (43).

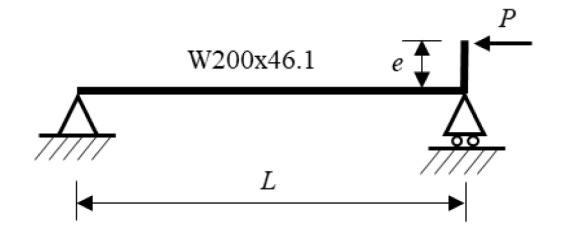


Fig. 3. Eccentrically loaded beam-column..

- 4. Calculate the generalized stress resultant vector for each Gauss point (use generalized stress resultant shape functions) as S^{i+1} = $N_{D1}P^{i+1}$.
- 5. Update section deformation d^{i+1} derived from the interpolated generalized stress resultant vector using Eq. (54) as $d^{i+1} = d^i +$ $f[S^{i+1}-S^i_{\Sigma}].$
- 6. Send section deformation d^{i+1} to the fiber section function to update the uniaxial material properties, section stiffness matrix and generalized stress resultant vector S_{Σ}^{i+1} .
- 7. Calculate the auxiliary matrices using Gauss quadrature from Eqs. (51), (57), (58), (59), (61), (66), (67), (68), and (69).
- 8. Calculate the element internal resisting force vector using $P_{int}^{i+1} =$
- $G_{1}^{T}P_{s}^{i+1} + \int_{l_{0}} N_{D2}^{T} \left(\dot{d}^{i+1} d^{i+1}\right) dx + \left(G_{1} + M_{d} H_{12}\right)^{T} H_{11}^{-1} V^{i+1}.$ 9. Calculate element tangent stiffness matrix using $K_{b} = \left(K_{g} + G_{2}^{T} + G_{2} H_{22}\right) + \left(G_{1} + M_{d} H_{12}\right)^{T} H_{11}^{-1} \left(G_{1} + M_{d} H_{12}\right).$

Then the global tangent stiffness matrix and internal force vector may be obtained through corotational transformation according to Eqs. (12) and (13). At this time, the global solution can be computed, and a convergence test should be conducted. If the residual is smaller than the threshold, then the next increment may be commenced. Otherwise, the iterations should be continued.

4. Validation of formulation

Ten examples are shown here to demonstrate the ability of the new mixed elements. In examples 1-6 and 10, the material is assumed to be linear elastic. Examples 7-9 address both elastic and inelastic materials. Example 4 incorporates nonproportional loading, while the other examples are proportional load, and example 10 is a nonlinear dynamic structure, while the other examples incorporate static loading. These examples show that the new mixed element can simulate both geometric and material nonlinearity accurately. In the following examples, "DBxx" indicates using xx number of a new displacement-based element with membrane locking remedied as presented in Du and Hajjar [33], while "MBxx" indicates using xx number of the mixed formulation elements presented in this work. The number of cross-sectional fibers used in the examples has been selected to be computationally efficient and sufficient to ensure accuracy in the results.

4.1. Eccentrically-loaded beam-column

This example is about a problem investigated by Neuenhofer and Filippou [13] and Alemdar [1], where a simply supported beam-column is subjected to an eccentric axial load (see Fig. 3). The beam-column has a length of L = 6668.52 mm and the eccentricity is e = 20.83 mm. The beam-column is in strong axis bending with a bending stiffness EI and the axial load is $P = 8EI/L^2$. The material properties are: Young's modulus E = 199,948 MPa and Poisson's ratio v = 0.3.

In this example, 1 displacement-based element with membrane locking remedied and 1 mixed element are used initially to analyze this

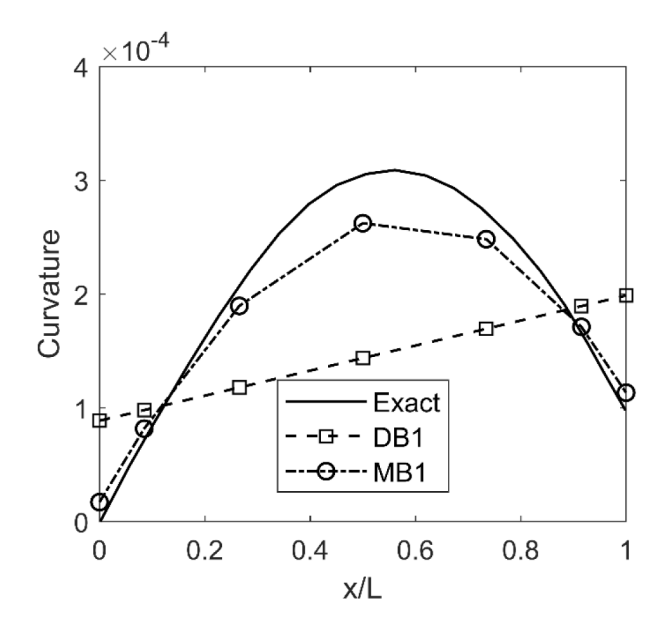


Fig. 4. Curvature field along the member (1 element).

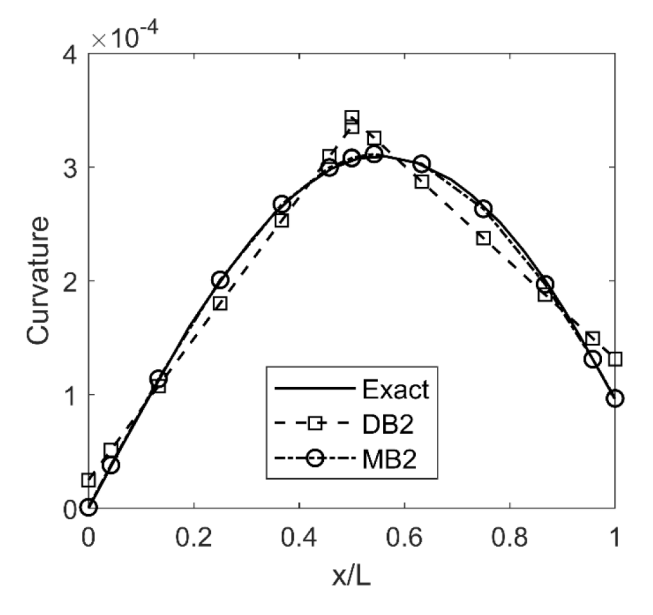


Fig. 5. Curvature field along the member (2 elements).

problem with elastic material. Fig. 4 compares the exact curvature field along the member with that at the Gauss integration points calculated from the displacement-based and mixed elements. It is shown that the displacement-based element exhibits a linear curvature field due to the cubic shape functions for transverse deflections. On the contrary, the mixed element is able to represent a nonlinear curvature field due to the independently interpolated force fields and displacement fields. Equilibrium is satisfied in a weighted average sense for the displacement-based element, while it is satisfied at each Gauss integration point within the mixed element. This problem is then analyzed using 2 elements with the results shown in Fig. 5. The curvature field of the displacement-based element includes two linear sections with a discontinuity at the connection point, while the mixed element yields a better approximation for the nonlinear curvature field with no discontinuity. In the above analysis, a seven-point Gauss-Lobatto integration rule is used for each element with 24 fibers in the cross section.

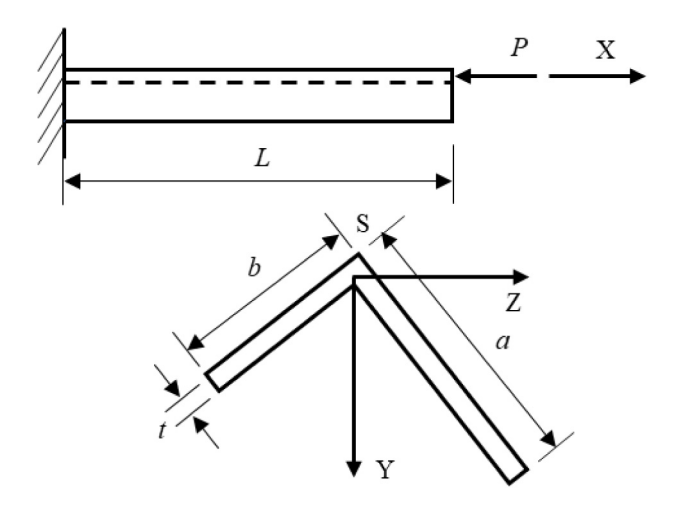


Fig. 6. Angle cantilever subjected to an eccentric axial load.

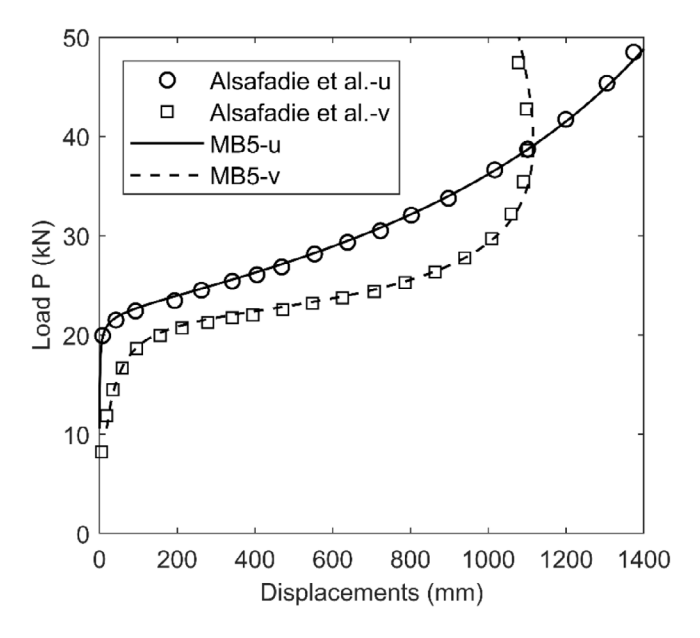


Fig. 7. Load-displacements u and v curves of the angle cantilever.

4.2. Angle cantilever subjected to an eccentric axial load

The example, studied numerically by several researchers [4,18,23], addresses a cantilever with asymmetric angle section subjected to an eccentrically applied axial load P. The cantilever is fixed at the left end (see Fig. 6). The axial load P is assumed to act through the shear center of the free end. As shown in Fig. 6, the geometric and material properties of the cantilever are: L=1,400 mm, a=76 mm, b=51 mm, t=6.5 mm, Young's modulus E=193,050 MPa and Poisson's ratio v=0.3. The load-deflection curves of the present study together with the results of Alsafadie et al. [23] are plotted in Fig. 7, in which the axial displacement u and lateral displacement v in Y direction are presented. As seen in this figure, five new mixed elements in the present study are enough to obtain relatively accurate results, while Alsafadie et al. [23] utilized 10 mixed elements to get similar results. In the analysis, a two-point Gauss-Lobatto integration rule is used for each element with 25 fibers in the cross section.

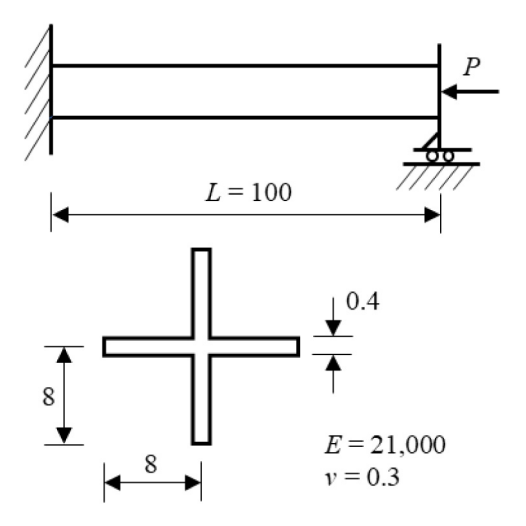
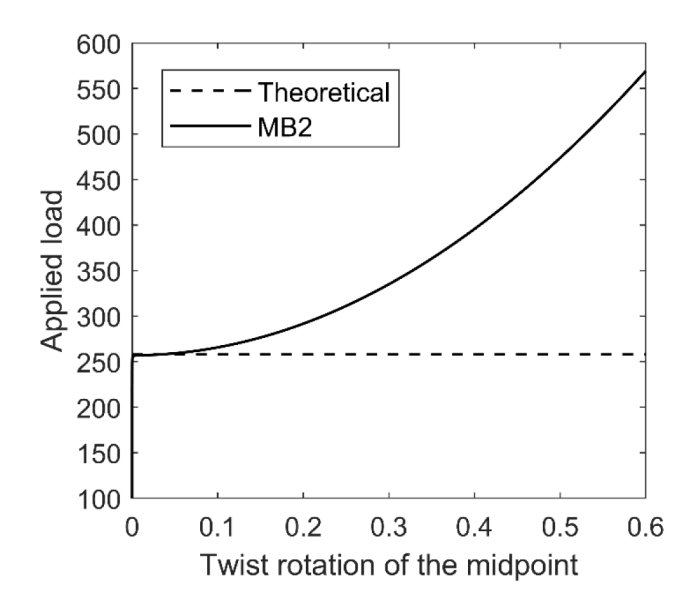


Fig. 8. Torsional buckling of a cruciform beam section.



 $\textbf{Fig. 9.} \ \ \textbf{Torsional buckling: axial load-twist rotation curves.}$

4.3. Torsional buckling

This example studies the axial-torsional buckling of a beam with a cruciform cross section. Fig. 8 illustrates the boundaries, the geometry properties and the material properties of the beam. All DOFs are fixed at the left end, and only the axial displacement is permitted at the right end. The axial compressive force P is applied at the centroid of the right end. This example was studied theoretically and numerically by Le Corvec [34]. By adopting the theory shown in Timoshenko and Gere [35], Le Corvec [34] calculated the theoretical buckling load of the beam as 258. The buckling analysis results in this study using 2 mixed elements are presented in Fig. 9 with the theoretical buckling load. It can be concluded that the buckling load of the element developed in this work agrees well with the theoretical value of 258. In the analysis, a five-point Gauss-Lobatto integration rule is used for each element with 25 fibers in the cross section.

4.4. Flexural-torsional interaction

This example investigates the torsional stiffness of an angle section under different bending moments at the ends. The experiments were

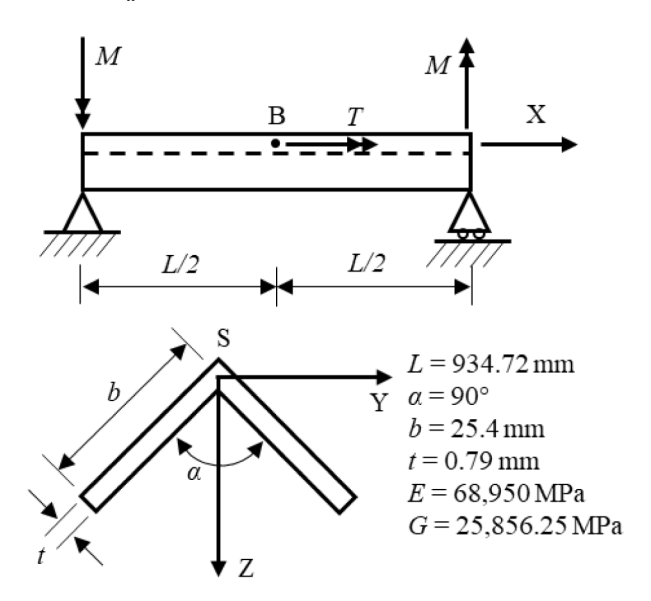


Fig. 10. Simply supported angle bar subjected to end moments and mid-span torque.

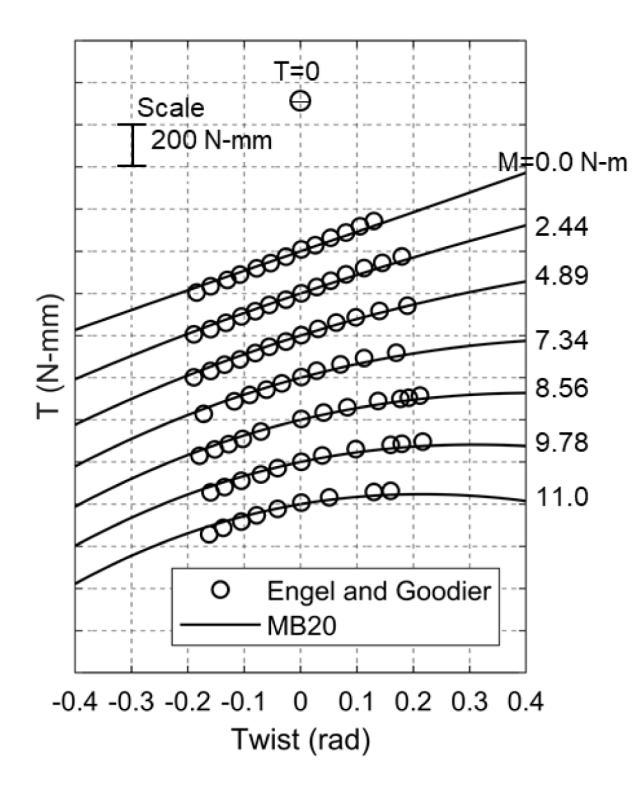


Fig. 11. Torque versus twist in the mid-span.

conducted on simply supported angle bars by Engel and Goodier [36]. The geometrical and material properties are shown in Fig. 10. The end moments were applied in the plane perpendicular to the plane of symmetry. In the present study, this experiment is simulated using 20 mixed elements. The comparison of the torque-twist curves under different bending moments from the simulations and experiments are shown in Fig. 11 with very good agreement. In the analysis, a five-point Gauss-Lobatto integration rule is used for each element with 25 fibers in the cross section.

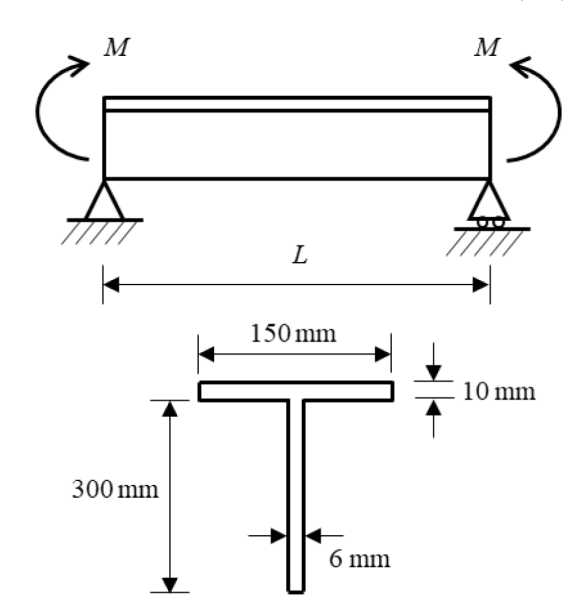


Fig. 12. Simply supported tee beam subjected to a uniform moment.

Table 1
Buckling loads of simply supported tee beams subjected to pure bending.

Beam length (L)	Buckling loads (kN-m)			
	Theory [37]	Mixed element		
6 m	57.8	56.0		
9 m	31.4	31.0		
12 m	21.1	21.0		

4.5. Lateral-torsional buckling of simply supported tee beams

The elastic buckling of simply supported tee beams under a uniform moment was investigated by Kitipornchai and Wang [37], as shown in Fig. 12. For this problem, a closed form analytical solution for the critical buckling moment is given by Kitipornchai and Wang [37]. For the section properties shown in Fig. 12, buckling loads are obtained for three different beam lengths using 20 the newly developed mixed elements. In this example, Young's modulus and shear modulus of elasticity are 200,000 MPa and 80,000 MPa, respectively. The comparison of the results from the present study and Kitipornchai's theoretic equation are presented in Table 1. It is shown that the lateral-torsional buckling loads are accurately predicted by the mixed elements. In the analysis, a five-point Gauss-Lobatto integration rule is used for each element with 23 fibers in the cross section.

4.6. Buckling of a right-angled frame subjected to an end load

The right-angled frame illustrated in Fig. 13 was studied by many researchers [1,5,7,38]. The load *P* is applied in the X-direction at the member tip with a very small perturbation load of 0.0002 N in the *Z*-direction at the tip to induce buckling artificially. The problem is solved using both the displacement-based element with membrane locking remedied and the mixed element. The computed response of the applied load *P* and the tip deflection in *Z*-direction is plotted in Fig. 14 together with the results of Alemdar [1] and Simo and Vu-Quoc [38]. It is shown that only 10 elements (5 for each member) are enough to obtain an accurate response. As shown in Du and Hajjar [33], more than 20 elements are required to get similar results if the displacement-based element with membrane locking is used. Since the results from the mixed element and the displacement-based element with membrane

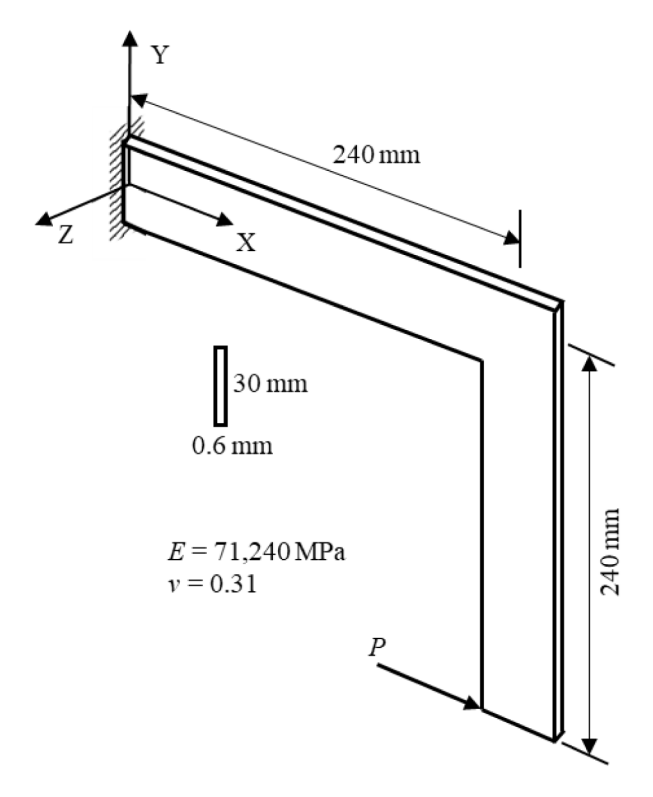


Fig. 13. Right-angled frame subjected to an end load.

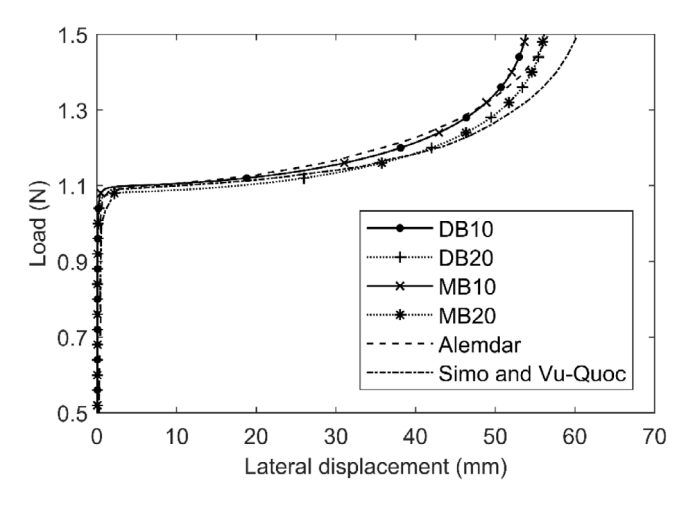


Fig. 14. Load/tip Z-displacement for the right-angled frame.

locking remedied are almost the same, it can be accepted that the mixed element is free of membrane locking. In the analysis, a five-point Gauss-Lobatto integration rule is used for each element with 36 fibers in the cross section. Six layers of fibers are adopted in the Z-direction to model the out-of-plane buckling behavior.

4.7. Flexural-torsional buckling of a tee beam

This example studies flexural-torsional buckling of a tee beam under axial load as shown in Fig. 15 considering both elastic and inelastic material. The left end of the beam is fixed and only the axial displacement is allowed at the right end. A compressive axial force P is applied at the shear center of the right end with a small perturbation force F = P/1000 introduced at the midspan point in the Z-direction. Battini and Pacoste [3] conducted numerical investigation on this example with the following geometrical and material properties: L = 1,800, h = b = 60,

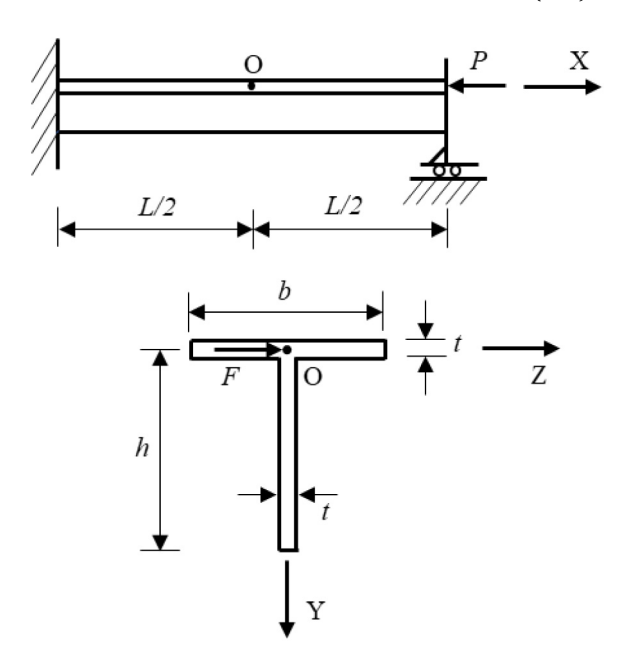


Fig. 15. Flexural-torsional buckling of a tee beam.

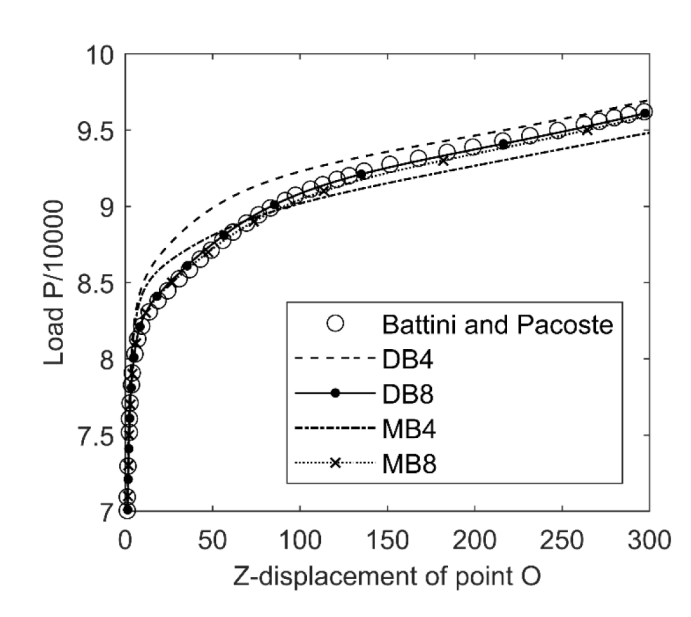


Fig. 16. Load/Z-displacement of point O curve (elastic case).

t=6, Young's modulus E=70,000, Poisson's ratio v=0.33, and yielding stress $F_y=20$. For the inelastic case, a bilinear elastic-plastic constitutive relation is assumed using a post-yield strain hardening modulus $E_{\rm t}=E/5$. In the present research, 4 and 8 displacement-based and mixed elements with 228 fibers in the cross section are used to simulate the buckling and yielding behavior. Here a five-point Gauss-Lobatto integration rule is used for each element. Note that Battini and Pacoste [3] used 40 elements and 288 cross-sectional fibers in their simulation.

A graph of load vs. Z-displacement of point O for the elastic and inelastic cases are shown in Fig. 16 and Fig. 17, respectively. The agreement between the present simulation results and the results of Battini and Pacoste [3] is very good, but fewer elements are needed for the present displacement-based and mixed element. In addition, the mixed element provides improved results as compared to the displacement-based element with the same number of elements.

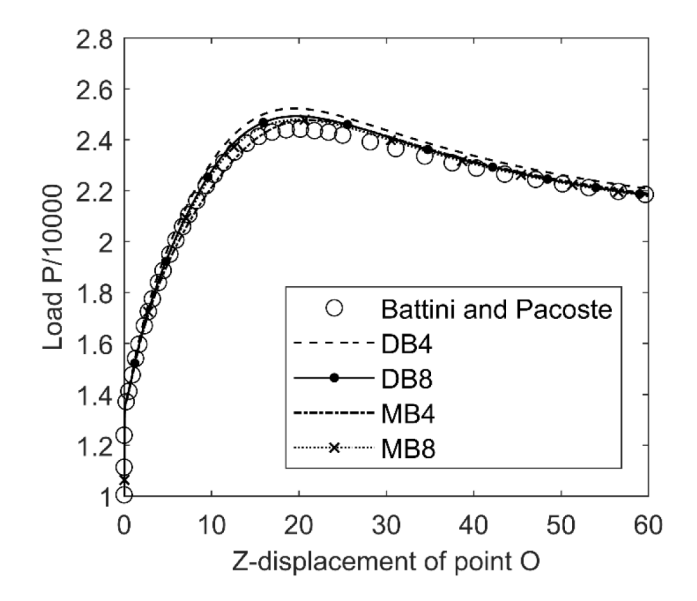


Fig. 17. Load/Z-displacement of point O curve (inelastic case).

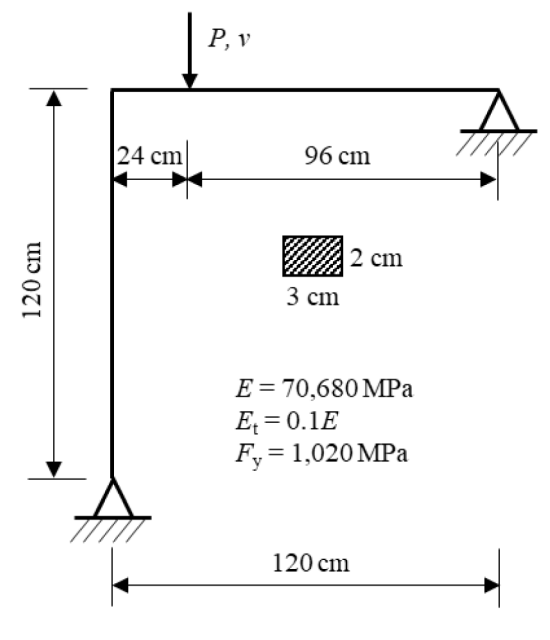


Fig. 18. Lee's frame.

4.8. Lee's frame

The frame represented in Fig. 18 was investigated by Lee et al. [39] and other authors. Several authors numerically studied this example only assuming linear elastic material [38,40,41]. de Souza [7] and Cichoń [42] analyzed this example for both elastic and inelastic cases. In the present study, the bilinear elasto-plastic material model with kinematic hardening proposed by de Souza [7] is adopted (see Fig. 18 for the material properties). Weak axis bending is used for both the horizontal and vertical members.

The frame is analyzed using both the displacement-based element with membrane locking remedied and the mixed element. Figs. 19 and 20 illustrate the results from the present study and those from de Souza [7]. It is shown that with the same number of elements (e.g. DB4 and MB4 in the figures), the mixed element can produce more accurate results than the displacement-based element with membrane locking remedied. This is because that the mixed element can represent

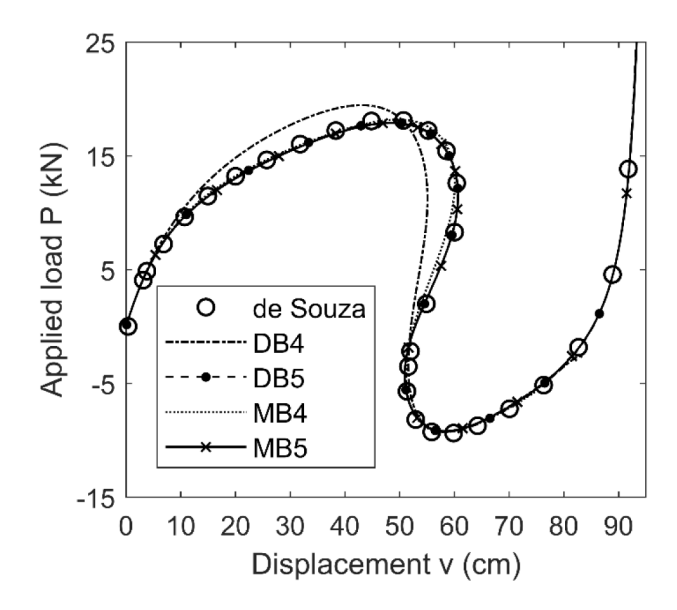


Fig. 19. Equilibrium path for Lee's frame (elastic).

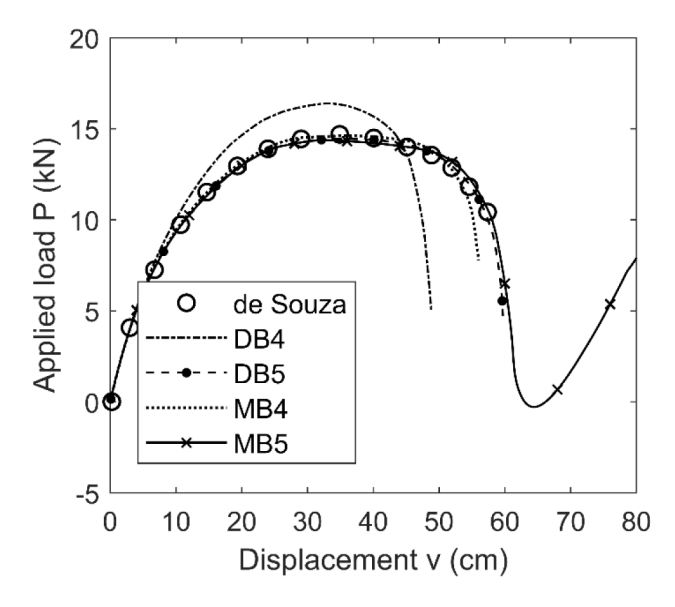


Fig. 20. Equilibrium path for Lee's frame (inelastic).

nonlinear curvature within an element more accurately. Note that for DB4 and MB4, three elements are used for the horizontal member and one element is used for the vertical member, while for DB5 and MB5, three elements are used for the horizontal member and two elements are used for the vertical member. In the analysis, a five-point Gauss-Lobatto integration rule is used for each element with 16 fibers in the cross section.

4.9. Buckling of single angle columns

This example compares the results of numerical and experimental investigations of the buckling behavior of single angle columns. Equalleg (L76 \times 76 \times 9.5 mm) and unequal-leg (L127 \times 76 \times 9.5 mm) angles, made of ASTM A36 steel, with different slenderness ratios (approximately 50, 100, 150) are used to study elastic and inelastic buckling responses. Al-Sayed and Bjorhovde [43] conducted experiments on three full-size simply supported columns for each section. Material property tests and residual stress measurements were also performed before the column tests. The measured yield stresses of

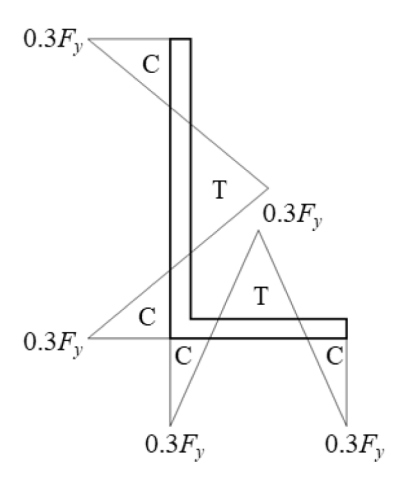


Fig. 21. Standard residual stress distribution for angle sections (F_y is the yielding stress).

sections L76 \times 76 \times 9.5 and L127 \times 76 \times 9.5 are 322 MPa and 311 MPa, respectively. The measured residual stresses were found to have a lack of equilibrium due to the coarseness of the discretization of the cross section and inaccuracies in the strain measurement; therefore, Al-Sayed and Bjorhovde [43] revised the measured residual stresses to obtain the balanced residual stresses.

In the present study, all the six experiments are simulated using the new mixed element. Bilinear stress-strain curve is assumed with the tested yielding stresses. Since Al-Sayed and Bjorhovde [43] did not provide strain hardening ratios in the material property tests, the average strain hardening modulus of A36 steel provided by Salmon et al. [44] are adopted in the simulation. Both the balanced residual stresses provided by Al-Sayed and Bjorhovde [43], the standard residual stresses shown in Fig. 21, and the no residual stress case are used to see the impact of residual stress pattern on the buckling response. Fig. 22 shows the relationship between twist at mid-length and the axial load ratio for the column with section L127 \times 76 \times 9.5 and slenderness L/r = 140.29, where P is the applied axial load and P_v is the yield load. It can be seen that the residual stress pattern has a significant influence on the buckling response of the column. The buckling loads calculated from the numerical models together with those obtained from the experiments are listed in Table 2. In general, the numerical results of the buckling loads have good agreement with the experimental results. Comparison of the buckling loads computed with balanced residual stress and standard residual stress demonstrates that the residual stress pattern can impact the buckling loads dramatically. Therefore, the discrepancies between the experimental and numerical results may come from the measurement of residual stress and the digitization of the residual stress distribution from very poor-quality figures provided by Al-Sayed and Bjorhovde [43]. Moreover, only one measurement was performed for each section, which may not represent the residual stress patterns for all the three columns with the same section size. In the analysis, a five-point Gauss-Lobatto integration rule is used for each element with 25 fibers in the cross section.

4.10. Nonlinear dynamic analysis of a cantilever with tee section

Le et al. [45] investigated the nonlinear dynamic response of a cantilever with a tee section as given in Fig. 23. The material properties are: E=210,000 MPa, v=0.3, and $\rho=7850$ kg/m³. All DOFs are fixed at the left end. Two time-variant loads ($P_y=-50P(t)$, $P_z=25P(t)$) are applied to point O of the right end section with the time history of P(t) shown in Fig. 24. Forty mixed elements with the lumped mass matrix are used to model this cantilever. The tee section is divided into 18 fibers and 5 Gauss-Lobatto integration points are used

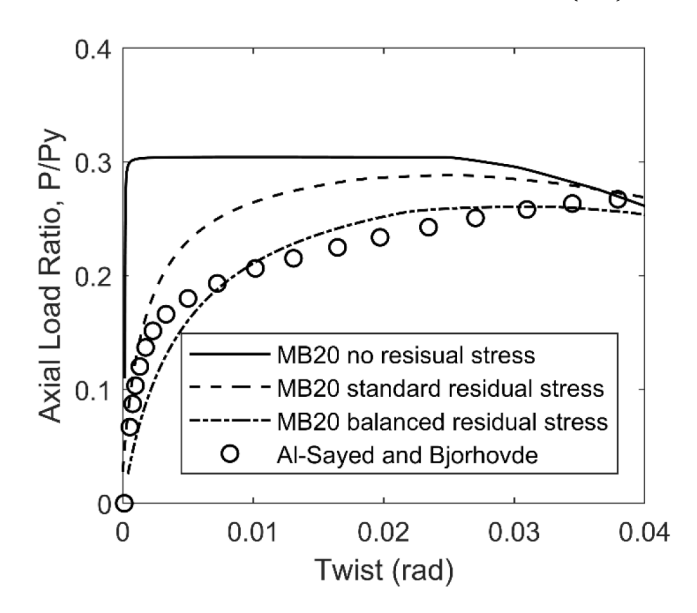


Fig. 22. Twist at mid-length vs. axial load ratio for a column with section L127 \times 76 \times 9.5 and slenderness L/r = 140.29.

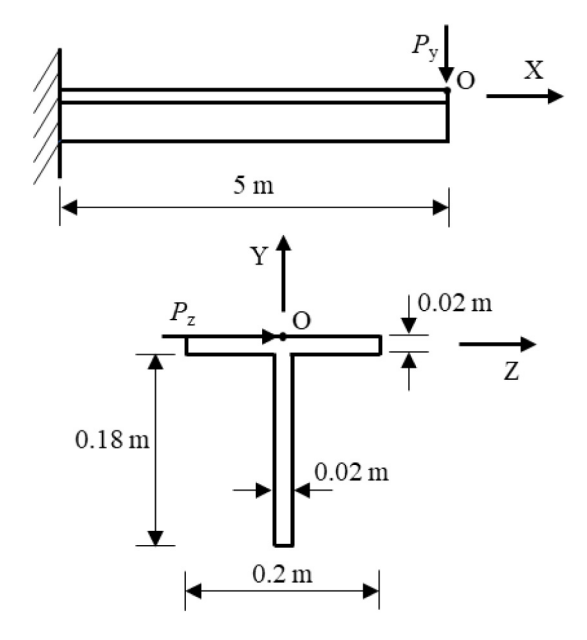


Fig. 23. Cantilever with a tee section.

for each element. The time step for this analysis is 0.001 s, and damping is not considered. The Z-displacement time history of the right end centroid is plotted in Fig. 25 together with the results provided by Le et al. [45], including the results of 40 corotational beam elements, 80 Abaqus B31OS elements and 2880 Abaqus isoparametric 20-node solid elements. The displacement time histories obtained from different elements agree well. The small discrepancies should be induced by the fact that a lumped mass matrix is adopted in this research while a consistent mass matrix is used by Le et al. [45].

5. Conclusions

A mixed beam element has been developed and implemented in the OpenSees software for geometric and material nonlinear analysis of structural members composed of cross sections with no significant torsional warping. The corotational total Lagrangian framework is utilized to model the geometric nonlinear behavior including flexural,

Table 2Comparison of the buckling loads obtained from experiments and numerical simulations.

Section	Slenderness L/r	P_{y} (kN)	Experimental buckling load (kN)	Numerical buckling load with balanced residual stress (kN)	Numerical buckling load with standard residual stress (kN)
$76 \times 76 \times 9.5$	49.50	438.02	418.58	394.51	361.51
$76 \times 76 \times 9.5$	103.27	438.02	230.42	211.29	193.54
$76 \times 76 \times 9.5$	156.30	438.02	103.73	96.62	91.68
$127\times76\times9.5$	44.34	573.78	510.66	509.46	500.16
$127\times76\times9.5$	99.77	573.78	303.37	261.96	291.98
$127\times76\times9.5$	140.29	573.78	161.83	149.59	165.43

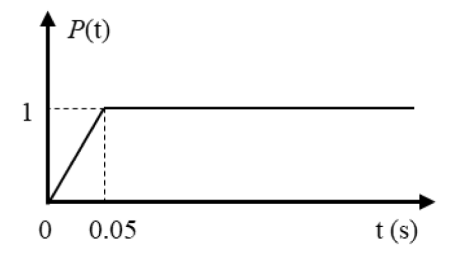


Fig. 24. Time history of P(t).

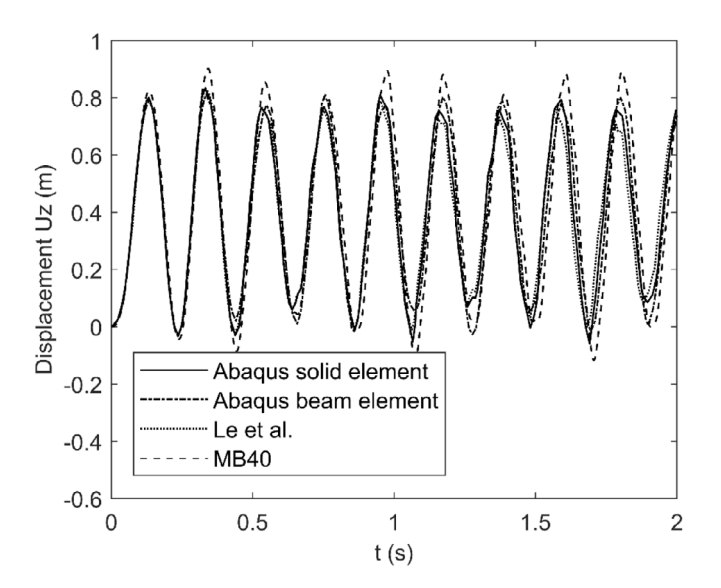


Fig. 25. Time histories of the Z-displacement (Uz) of the right end centroid.

flexural-torsional and axial-torsional buckling. In order to deal with the noncoincident centroid and shear center for asymmetric sections, a special basic coordinate system is adopted with displacements and rotations defined with different reference points, and then all DOFs are transformed to the shear center. The fiber section method with uniaxial stress-strain models is used to consider material nonlinearity. In the basic system, a two-field mixed element is formulated with the help of the Hellinger-Reissner functional and displacement and generalized stress resultant shape functions are derived from the nonlinear equilibrium equations so that the P - δ effects are considered in the interpolated stress resultants. Numerical examples show that the mixed element does not have a membrane locking issue. Furthermore, as demonstrated by the numerical examples, the use of mixed element can reduce the number of elements needed to model nonlinear curvature problems compared

with a comparable displacement-based element with membrane locking remedied. This is because the displacement-based element can only represent a linear curvature field exactly within an element, while the mixed element can model a nonlinear curvature field due to the stress resultant fields included in the element formulation and the element state determination which ensure that the equilibrium equations are satisfied section by section along the element.

CRediT authorship contribution statement

Xinlong Du: Methodology, Software, Validation, Writing - original draft. **Jerome F. Hajjar:** Conceptualization, Writing - review & editing.

Declaration of competing interest

The authors declare that they have no known competing financial interests or personal relationships that could have appeared to influence the work reported in this paper.

Acknowledgment

The material presented in this paper is based upon work supported by National Science Foundation under Grant No. CRISP-1638234 and Northeastern University, Boston, Massachusetts. This support is gratefully acknowledged.

References

- B.N. Alemdar, Distributed plasticity analysis of steel building structural systems (Ph.D. Thesis), Georgia Institute of Technology, Atlanta, Georgia, USA, 2001.
- [2] J.-M. Battini, C. Pacoste, Co-rotational beam elements with warping effects in instability problems, Comput. Methods Appl. Mech. Engrg. 191 (17–18) (2002) 1755–1789.
- [3] J.-M. Battini, C. Pacoste, Plastic instability of beam structures using co-rotational elements, Comput. Methods Appl. Mech. Engrg. 191 (51–52) (2002) 5811–5831.
- [4] H.H. Chen, W.Y. Lin, K.M. Hsiao, Co-rotational finite element formulation for thin-walled beams with generic open section, Comput. Methods Appl. Mech. Engrg. 195 (19–22) (2006) 2334–2370.
- [5] M.A. Crisfield, A consistent co-rotational formulation for non-linear, three-dimensional, beam-elements, Comput. Methods Appl. Mech. Engrg. 81 (2) (1990) 121, 150
- [6] M.A. Crisfield, Non-Linear Finite Element Analysis of Solids and Structures -Advanced Topics, John Wiley & Sons, Chichester, United Kingdom, 1997.
- [7] R.M. de Souza, Force-based finite element for large displacement inelastic analysis of frames (Ph.D. Thesis), University of California, Berkeley, Berkeley, California, USA, 2000.
- [8] K.M. Hsiao, W.Y. Lin, A co-rotational formulation for thin-walled beams with monosymmetric open section, Comput. Methods Appl. Mech. Engrg. 190 (8–10) (2000) 1163–1185.
- [9] K. Mattiasson, A. Bengtsson, A. Samuelsson, On the accuracy and efficiency of numerical algorithms for geometrically nonlinear structural analysis, in: P.G. Bergan, K.J. Bathe, W. Wunderlich (Eds.), Europe-US Symposium on Finite Element Methods for Nonlinear Problems, Springer-Verlag, Trondheim, Norway, 1085

- [10] B. Izzuddin, D.L. Smith, Large-displacement analysis of elastoplastic thin-walled frames. I: formulation and implementation, J. Struct. Eng. 122 (8) (1996) 905–914
- [11] B. Izzuddin, D.L. Smith, Large-displacement analysis of elastoplastic thin-walled frames. II: verification and application, J. Struct. Eng. 122 (8) (1996) 915–925.
- [12] S. El-Tawil, G.G. Deierlein, Nonlinear analysis of mixed steel-concrete frames. I: Element formulation, J. Struct. Eng. 127 (6) (2001) 647–655.
- [13] A. Neuenhofer, F.C. Filippou, Geometrically nonlinear flexibility-based frame finite element, J. Struct. Eng. 124 (6) (1998) 704–711.
- [14] B.N. Alemdar, D.W. White, Displacement, flexibility, and mixed beam-column finite element formulations for distributed plasticity analysis, J. Struct. Eng. 131 (12) (2005) 1811–1819.
- [15] P.K.V. Nukala, D.W. White, A mixed finite element for three-dimensional nonlinear analysis of steel frames, Comput. Methods Appl. Mech. Engrg. 193 (23–26) (2004) 2507–2545.
- [16] C. Tort, J.F. Hajjar, Mixed finite element for three-dimensional nonlinear dynamic analysis of rectangular concrete-filled steel tube beam-columns, J. Eng. Mech. 136 (11) (2010) 1329–1339.
- [17] F.G. Al-Bermani, S. Kitipornchai, Elasto-plastic large deformation analysis of thin-walled structures, Eng. Struct. 12 (1) (1990) 28–36.
- [18] S. Chan, S. Kitipornchai, Geometric nonlinear analysis of asymmetric thin-walled beam-columns, Eng. Struct. 9 (4) (1987) 243–254.
- [19] S. Kitipornchai, S. Chan, Nonlinear finite element analysis of angle and tee beam-columns, J. Struct. Eng. 113 (4) (1987) 721–739.
- [20] S.-W. Liu, W.-L. Gao, R.D. Ziemian, Improved line-element formulations for the stability analysis of arbitrarily-shaped open-section beam-columns, Thin-Walled Struct. 144 (2019) 106290.
- [21] S.-W. Liu, R.D. Ziemian, L. Chen, S.-L. Chan, Bifurcation and large-deflection analyses of thin-walled beam-columns with non-symmetric open-sections, Thin-Walled Struct, 132 (2018) 287–301
- [22] Rinchen, G.J. Hancock, K.J. Rasmussen, Geometric and material nonlinear analysis of thin-walled members with arbitrary open cross-section, Thin-Walled Struct. 153 (2020) 106783.
- [23] R. Alsafadie, M. Hjiaj, J.-M. Battini, Corotational mixed finite element formulation for thin-walled beams with generic cross-section, Comput. Methods Appl. Mech. Engrg. 199 (49–52) (2010) 3197–3212.
- [24] R. Alsafadie, M. Hjiaj, J.-M. Battini, Three-dimensional formulation of a mixed corotational thin-walled beam element incorporating shear and warping deformation, Thin-Walled Struct. 49 (4) (2011) 523–533.
- [25] F. McKenna, M.H. Scott, G.L. Fenves, Nonlinear finite-element analysis software architecture using object composition, J. Comput. Civ. Eng. 24 (1) (2010) 95–107
- [26] G. Hancock, Portal frames composed of cold-formed channel- and Z-sections, Steel Framed Structures - Stability and Strength (2005) 230–264.
- [27] N.S. Trahair, Flexural-Torsional Buckling of Structures, first ed., CRC Press, Boca Raton. 1993.

- [28] K. Rasmussen, Bifurcation of locally buckled members, Thin-Walled Struct. 28 (2) (1997) 117–154.
- [29] N. Trahair, Nonlinear elastic nonuniform torsion, J. Struct. Eng. 131 (7) (2005) 1135–1142.
- [30] P.K.V. Nukala, D.W. White, Variationally consistent state determination algorithms for nonlinear mixed beam finite elements, Comput. Methods Appl. Mech. Engrg. 193 (33–35) (2004) 3647–3666.
- [31] M.D. Denavit, J.F. Hajjar, Nonlinear seismic analysis of circular concrete-filled steel tube members and frames, J. Struct. Eng. 138 (9) (2012) 1089–1098.
- [32] C. Tort, J.F. Hajjar, Reliability-based performance-based design of rectangular concrete-filled steel tube (RCFT) members and frames, Structural Engineering Report No. ST-07-1, Department of Civil Engineering, University of Minnesota, Minneapolis, Minnesota, USA (2007).
- [33] X. Du, J.F. Hajjar, Three-dimensional nonlinear displacement-based beam element for members with angle and tee sections, Eng. Struct. 239 (2021) 112239.
- [34] V. Le Corvec, Nonlinear 3d frame element with multi-axial coupling under consideration of local effects (Ph.D. Thesis), University of California, Berkeley, Berkeley, California, USA, 2012.
- [35] S. Timoshenko, J.M. Gere, Theory of Elastic Stability, second ed., McGraw-Hill, New York, New York, USA, 1961.
- [36] H. Engel, J. Goodier, Measurements of torsional stiffness changes and instability due to tension, compression, and bending, J. Appl. Mech.-Trans. ASME 20 (4) (1953) 553–560.
- [37] S. Kitipornchai, C. Wang, Lateral buckling of tee beams under moment gradient, Comput. Struct. 23 (1) (1986) 69–76.
- [38] J.C. Simo, L. Vu-Quoc, A three-dimensional finite-strain rod model. Part II: Computational aspects, Comput. Methods Appl. Mech. Engrg. 58 (1) (1986) 79–116.
- [39] S.-L. Lee, F.S. Manuel, E.C. Rossow, Large deflections and stability of elastic frame, J. Eng. Mech. Div. 94 (2) (1968) 521–548.
- [40] C. Pacoste, A. Eriksson, Beam elements in instability problems, Comput. Methods Appl. Mech. Engrg. 144 (1–2) (1997) 163–197.
- [41] H. Chen, G.E. Blandford, Work-increment-control method for non-linear analysis, Internat. J. Numer. Methods Engrg. 36 (6) (1993) 909–930.
- [42] C. Cichoń, Large displacements in-plane analysis of elastic-plastic frames, Comput. Struct. 19 (5–6) (1984) 737–745.
- [43] S.H. Al-Sayed, R. Bjorhovde, Experimental study of single angle columns, J. Construct. Steel Res. 12 (2) (1989) 83–102.
- [44] C.G. Salmon, J.E. Johnson, F.A. Malhas, Steel Structures Design and Behaviour, fifth ed., Pearson Pretice Hall, Upper Saddle River, New Jersey, US, 2009.
- [45] T.-N. Le, J.-M. Battini, M. Hjiaj, Corotational formulation for nonlinear dynamics of beams with arbitrary thin-walled open cross-sections, Comput. Struct. 134 (2014) 112–127.